Structural Engineering and Mechanics, Vol. 35, No. 3 (2010) 315-333
DOI: http://dx.doi.org/10.12989/sem.2010.35.3.315

Nonlinear finite element analysis of circular concrete-filled steel tube structures

Tengfei Xu, Tianyu Xiang*, Renda Zhao and Yulin Zhan

Department of Bridge Engineering, Southwest Jiaotong University, Chengdu 610031, P.R. China

(Received April 15, 2009, Accepted January 27, 2010)

Abstract. The structural behaviors of circular concrete filled steel tube (CFT) structures are investigated by nonlinear finite element method. An efficient three-dimensional (3D) degenerated beam element is adopted. Based on those previous studies, a modified stress-strain relationship for confined concrete which introduces the influence of eccentricity on confining stress is presented. Updated Lagrange formulation is used to consider the geometrical nonlinearity induced by large deformation effect. The nonlinear behaviors of CFT structures are investigated, and the accuracy of the proposed constitutive model for confined concrete is mainly concerned. The results demonstrate that the confining effect in CFT elements subjected to combining action of axial force and bending moment is far sophisticated than that in axial loaded columns, and an appropriate evaluation about this effect may be important for nonlinear numerical simulation of CFT structures.

Keywords: concrete-filled steel tube; nonlinear finite element analysis; degenerated beam element; updated lagrange formulation.

1. Introduction

Concrete-filled steel tube, which combines the advantages of steel and concrete, has attracted more and more attentions in civil engineering during the past four decades. First, the steel tube serves as a form for casting of core concrete, which results in reduction of cost and improvement of construction efficiency. Moreover, compared with hollow steel tube, concrete filling may prevent bulking of steel tube, and the stability of compressive element can be improved enormously. Among all these advantages, the most attractive merit of CFT is that the element exhibits excellent compressive resistance capacity, ductility, and energy dissipation ability due to the confining pressure provided by steel tube. Owing to those distinctive merits, CFT has been demonstrated as a suitable structural element for building columns, bridge piers, and arch ribs through worldwide engineering practices.

A great amount of significant research works have been continuously contributed to this subject. In those previous researches, experimental studies have played a key role in establishment of the general theory of CFT. Compared with experimental method, numerical approach is more economical and effective, which may be capable to simulate many experimentally unmanageable

*Corresponding author, Professor, E-mail: tyxiang@home.swjtu.edu.cn

cases. Moreover, through combing experimental and numerical approach, a more clear inspection about mechanical nature can be expected. Strip method is the most commonly adopted numerical method to analysis the resistance and ductility of CFT members (Fujimoto *et al.* 2004, Han 2004). One-dimensional stress-strain relationship is generally used in the strip method, and the confining effect is considered through modifying the peak stress and strain of constitutive curve of common concrete. Another choice of numerical method is nonlinear finite element analysis. In recent published literatures, nonlinear finite element analysis of CFT structures with three-dimensional solid element has been widely carried with commercial FEM package (Huang *et al.* 2002, Hu *et al.* 2003, Hu *et al.* 2005, Gupta *et al.* 2007). With three-dimensional solid element, the nonlinear FEM analysis can simulate such complex structural behaviors as bond-slip between steel and concrete, confining effect under sophisticated stress states, buckling of steel tube and so on, which can obtain a comprehensive insight about the basic mechanical nature of CFT structures. However, this approach is generally time-consuming especially for large complex structures. Moreover, with increment of scale of FEM model, strong nonlinearity caused by cracking and crushing of concrete, plasticity flow of steel, and so on, may bring some dilemmas for iteration convergence. To meet the requirement of nonlinear analysis for practical large CFT structures, three-dimensional beam-column finite element approach may be a comprised and effective way. In this approach, the elastic-plasticity behaviors of concrete and steel, which are the major nonlinearity factors of CFT structures, are emphasized. Such nonlinear resources as bond-slip between concrete and steel, buckling of tube, and so on are not considered. Some successful applications of this method can be found in the studies of Marques (2005) and Mirza *et al*. (1996).

In the present study, with three-dimensional degenerated beam element the nonlinear behaviors of CFT structures are investigated. The theory behind the degeneration technique is not new, and has been widely used in the formulation of shell and plate element (Ahmad *et al.* 1970, Worsak 1978, Parisch 1981). To formulate degenerated beam element, the hypothesis of plane section is adopted, and based on this hypothesis the three-dimensional displacement field can be described by nodal variables. Meanwhile, the strain-displacement equations of three-dimensional structure are retained. A nonlinear analysis program for concrete structures with degenerated beam element developed by Xiang *et al.* (2005) is adopted in the present study.

One-dimensional stress-strain relationship of concrete and steel is adopted in formulation of degenerated beam element. As aforementioned, to involve the confining effect, some modifications about stress-strain relationship of common concrete should be introduced. The current available works about stress-strain relationship of confined concrete are mainly based on the experimental results of axial compressive elements. However, for the structures under axial force and bending moment in combination, it should be noted that the confining effect may be more complicated. Through experimental investigation, Chen *et al.* (2002) found that for eccentrically loaded CFT column, with increment of load eccentricity, the confining stress applied on core concrete decreases gradually. Based on the experimental results, Chen *et al.* (2004) proposed a modified stress-strain relation for confined concrete which involves the influence of load eccentricity on confining pressure. Meanwhile, Hu *et al.* (2005) obtained a similar conclusion by three-dimensional nonlinear finite element analysis, and an empirical equation for confining pressure is presented.

For high-rise and long-span structures, geometrical nonlinearity should never be neglected. The secondary moment caused by large deformation may weak the confining effect of CFT structures. In the present study, the updated Lagrange formulation is employed to investigate the influence of geometrical nonlinearity on the structural behaviors of CFT members.

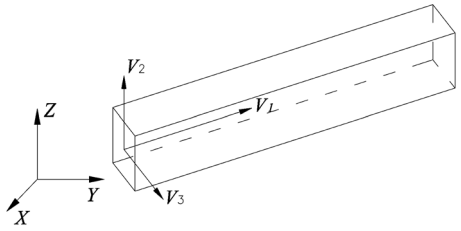

Fig. 1 The beam element

2. Formulation of degenerated beam element

2.1 Geometry and displacement field

The position of any point in the element illustrated in Fig. 1 can be given as

$$\vec{X} = \sum_{i=1}^{2} N_i(r)(\vec{X}_i + y'\vec{V}_2 + z'\vec{V}_3) \tag{1}$$

in which $\vec{X}$ is the coordinates of any point in the element, $\vec{X}_i$ is the coordinates of node i (i = 1~2). $\vec{V}_1, \vec{V}_2$ and $\vec{V}_3$ form the local orthogonal coordinate system shown in Fig. 1. y' and z' are the local coordinates in $\vec{V}_2$ and $\vec{V}_3$ directions, respectively. The interpolation function $N_i(r)$ is written as

$$N_i(r) = \frac{1}{2}(1 + r_i r) \tag{2}$$

where r_i is the isoparametric coordinate of node i.

The local orthogonal coordinate system shown in Fig. 1 can be constructed with the following way

$$\vec{V}_3 = \vec{V}_1 \times \vec{V}_2 \tag{3}$$

in which $\vec{V}_1$ is expressed as

$$\vec{V}_1 = ((x_2 - x_1)/L \quad (y_2 - y_1)/L \quad (z_2 - z_1)/L)^T \tag{4}$$

where L is the length of element. Then, with the given $\vec{V}_2, \vec{V}_3$ can be finally determined through Eq. (3).

The displacement field can be expressed in the form

$$\vec{U} = \sum_{i=1}^{2} N_i(r)[\vec{U}_i + \vec{U}_\alpha(y', z')] \tag{5}$$

where $\vec{U}$ is the displacement vector at any point in the element, $\vec{U}_i$ is the nodal displacement vector at node i, and $\vec{U}_\alpha(y', z')$ is relative nodal displacement produced by normal rotations. With the hypothesis of plane section, $\vec{U}_\alpha(y', z')$ can be expressed as

$$\begin{Bmatrix} u_i(\alpha) \\ v_i(\alpha) \\ w_i(\alpha) \end{Bmatrix} = \begin{bmatrix} \vec{V}_1 & \vec{V}_2 & \vec{V}_3 \\ \alpha'_{i1} & \alpha'_{i2} & \alpha'_{i3} \\ 0 & y' & z' \end{bmatrix} \tag{6}$$

where $\alpha'_{i1}, \alpha'_{i2}$ and α'_{i3} are the normal rotations about local axes of $\vec{V}_1, \vec{V}_2$ and $\vec{V}_3$. Considering displacement transformation relation, Eq. (6) can be written in terms of the normal rotations about global axes as

$$\begin{Bmatrix} u_i(\alpha) \\ v_i(\alpha) \\ w_i(\alpha) \end{Bmatrix} = \begin{bmatrix} 0 & y'n_2+z'n_3 & -y'm_2-z'm_3 \\ -y'n_2-z'n_3 & 0 & y'l_2+z'l_3 \\ y'm_2+z'm_3 & -y'l_2-z'l_3 & 0 \end{bmatrix} \begin{Bmatrix} \alpha_{i1} \\ \alpha_{i2} \\ \alpha_{i3} \end{Bmatrix} \tag{7}$$

in which $(l_2 \ m_2 \ n_2)^T$ and $(l_3 \ m_3 \ n_3)^T$ represent the direction cosine of $\vec{V}_2$ and $\vec{V}_3$ in global coordinate system. Then, Eq. (5) can be rewritten as

$$\vec{U} = \sum_{i=1}^{2} N_i(r)[\vec{U}_i + \Phi\vec{\alpha}_i] \tag{8}$$

where

$$\Phi = \begin{bmatrix} 0 & y'n_2+z'n_3 & -y'm_2-z'm_3 \\ -y'n_2-z'n_3 & 0 & y'l_2+z'l_3 \\ y'm_2+z'm_3 & -y'l_2-z'l_3 & 0 \end{bmatrix} \tag{9}$$

and $\vec{\alpha}_i$ is the normal rotation vector about global axes.

2.2 Geometrical nonlinearity and updated Lagrange formulation

Geometrical nonlinearity may occur in high-rise and long-span structures. Generally, the large displacement can be assumed to be a function of time, and the solutions of static and kinematic variables are given in a series of discrete time points, 0, Δt, $2\Delta t$..., t. To obtain the solutions for $t+\Delta t$, two different formulations, i.e., total Lagrange formulation and updated Lagrange formulation, can be employed. In total Lagrange formulation (T. L.), all static and kinematic variables are referred to the initial configuration. For updated Lagrange formulation (U. L), the procedure is similar with T. L., but all static and kinematic variables are referred to the last configuration (Parisch 1981). In the present paper, the U. L. formulation will be adopted.

For large displacement motion, the virtual work equation can be written as

$$\int_{V_0} S_{ij}\delta E_{ij} dV_0 = \int_{V_0} p_{0i}\delta u_i dV_0 + \int_{V_0} q_{0i}\delta u_i dA_0 \tag{10}$$

where S_{ij} and E_{ij} are the Kirchoff stress tensor and Green strain tensor, p_{0i} and q_{0i} mean body force and surface trace, u_i is the displacement tensor, and δ stands for variation.

Since U. L. formulation is referred to the last configuration, the Green strain should be given in an incremental form, which is defined as

$$\Delta E_{ij} = \Delta E_{ij}^{L} + \Delta E_{ij}^{N} = \frac{1}{2}\left(\frac{\partial \Delta u_i}{\partial x_j} + \frac{\partial \Delta u_j}{\partial x_i}\right) + \frac{1}{2}\frac{\partial \Delta u_k}{\partial x_i}\frac{\partial \Delta u_k}{\partial x_j} \tag{11}$$

in which ΔE_{ij}^{L} and ΔE_{ij}^{N} represent the linear and nonlinear strain, respectively. Substituting Eq. (8) into Eq. (11), the matrix form of linear and nonlinear strain-displacement relation can be derived

$$\Delta \vec{E}_L = [B]_L \Delta \vec{U} \tag{12}$$

$$\Delta \vec{E}_N = [\tilde{B}]_N \Delta \vec{U} \tag{13}$$

where $[B]_L$ and $[\tilde{B}]_N$ are the linear and nonlinear strain matrix, respectively. Using the virtual work equation given in Eq. (10), the geometrical stiffness matrix can be finally obtained, and the details about derivation procedure can be referred to the work of Bathe and Bolourchi (1980).

3. Constitutive model of material

To deal with material nonlinearity, the cross-section of degenerated beam element will be subdivided into a series of pieces, and the axial stress of every piece will be computed with one-dimensional constitutive model (Xiang *et al.* 2005). In this section, the uniaxial constitutive model of confined concrete and steel will be discussed.

3.1 Concrete

The experiment studies have revealed that confining effect of steel tube can increase compressive strength and ductility of concrete. Generally, to describe a complete curve of one-dimensional stress-strain relation of concrete confined by steel tube, several characteristic points should be identified. For the ascending branch, the compressive strength of confined concrete f_{cc}, the corresponding strain ε_{cc}, and the initial elastic modulus of concrete E_0 must be determined.

The compressive strength of confined concrete can be written in a simple and natural way as

$$f_{cc} = f_c + mf_{rp} \tag{14}$$

in which f_c is the compressive strength of unconfined concrete, f_{rp} is the average radial pressure acted on the core concrete, and m is an empirical constant which ranges from 4.0 to 6.0 (Hu *et al.* 2003) (In the present study, the value of m is assumed to be 4.2). It has been found that the average radial pressure f_{rp} apparently depends on the width-to-thickness ratio (D/t) (Hu *et al.* 2003). With experimental results (Hu *et al.* 2003, Schneider 1998, Susantha *et al.* 2001), an empirical formula of f_{rp} is presented through trial and error

$$\frac{f_{rp}}{f_y} = 0.3111\left(\frac{D}{t} - 2\right)^{-1.027} \tag{15}$$

The compressive strength of confined concrete given in Eq. (14) is established based on experimental studies of concentrically loaded columns. However, for eccentrically loaded CFT elements, the confining effect may be more sophisticated. Through experimental studies, Chen *et al.*

(2002) found that the confining stress of steel tube acted on core concrete decreases gradually with increment of load eccentricity. With experimental investigation and three-dimensional nonlinear finite element analysis, a similar phenomenon is also observed by Hu *et al.* (2005). In the present study, to take the effect of eccentricity on confining stress into account, a modified form of Eq. (14) is presented

$$f_{cc} = f_c + \alpha m f_{rp} \tag{16}$$

where α is a reduction parameter for radial pressure f_{rp}, which is defined as

$$\alpha = \begin{cases} \left(1 - \frac{2e}{D}\right)\exp\left(-\frac{2e}{D}\right) & \text{for} \quad \frac{2e}{D} < 1 \\ 0 & \text{for} \quad \frac{2e}{D} \geq 1 \end{cases} \tag{17}$$

where e represents the load eccentricity, and can be expressed as M/N (M and N represent the moment and axial force acted on the given section, respectively).

ε_{cc}, the strain corresponding to maximum stress f_{cc}, is defined in the present study as

$$\varepsilon_{cc} = \frac{f_{cc}}{f_c}\varepsilon_0 \tag{18}$$

in which ε_0 is the strain corresponding to maximum compressive stress f_c of unconfined concrete.

The confining effect does not exist in the initial elastic stage of loading due to the fact that Poisson ratio of concrete is lower than that of steel in this period. Therefore, it is assumed that the initial elastic modulus of confined concrete is equal to that of unconfined common concrete.

With the three parameters f_{cc}, ε_{cc}, and E_c, the stress-strain relation of confined concrete in the ascending branch can be described by Saenz equation (Saenz 1964)

$$\sigma = \frac{E_0 \varepsilon}{1 + \left(\frac{E_0}{E_{cs}} - 2\right)\left(\frac{\varepsilon}{\varepsilon_{cc}}\right) + \left(\frac{\varepsilon}{\varepsilon_{cc}}\right)^2} \tag{19}$$

where E_{cs} is secant modulus of concrete at peak stress point, which is given as f_{cc}/ε_{cc}.

For descending branch, with the experimental results (Gupt 2007, Hu 2003, Schneider 1998, Susantha 2001), an exponential degrading function illustrated in Fig. 2 is proposed

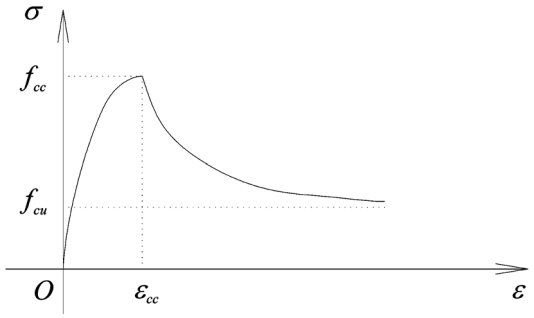

Fig. 2 Compressive stress-strain relation of steel tube confined concrete

$$\sigma = f_{cu} + (f_{cc} - f_{cu}) \cdot \exp\left(-k\frac{\varepsilon - \varepsilon_{cc}}{\varepsilon_{cc}}\right) \tag{20}$$

in which f_{cu} is the ultimate residual compressive stress shown in Fig. 2, and k is a parameter to describe the descending rate which is assumed to be 0.3 in the present study. f_{cu} is determined through the following equation

$$f_{cu} = \begin{cases} f_{cc} \cdot \left(\dfrac{0.1 f_y}{f_c}\right)^{0.1} & \text{for} \quad \dfrac{D}{t} \le 40 \\ f_{cc} \cdot \left(\dfrac{0.1 f_y}{f_c}\right)^{0.1} \cdot \left[\beta + (1-\beta) \cdot \exp\left(-\dfrac{\frac{D}{t} - 40}{40}\right)\right] & \text{for} \quad \dfrac{D}{t} \ge 40 \end{cases} \tag{21}$$

where β is an empirical parameter, which is assumed to be 0.6 in this paper.

The elastic-brittle model is adopted for tension of confined concrete, and the tensile strength is employed that of common concrete.

3.2 Steel

Under compressive load, axial compressive stress will be generated in steel tube. Meanwhile, owing to volume expansion of core concrete, the steel tube is also subjected to hoop tension stress. The biaxial stress state will occur in steel tube. With Von Mises criterion, the yield envelope of steel tube under biaxial stresses can be written as

$$\sigma_v^2 - \sigma_v \sigma_h + \sigma_h^2 = f_y^2 \tag{22}$$

in which σ_v is the axial stress of steel tube. With the assumption that hoop stress σ_h is assumed to be 0.1 f_y (Elremaily and Azizinamini 2002), the vertical yield stress of steel tube can be solved from Eq. (22)

$$f_{yv}^c \approx 0.95 f_y, \quad f_{yv}^t \approx 1.05 f_y \tag{23}$$

where f_{yv}^c and f_{yv}^t represent the axial compressive and tensile yield stress of steel tube, respectively.

One-dimensional perfect elasto-plastic constitutive model is adopted for steel tube. To improve the stability of numerical calculation, the modulus of steel after yield is assumed to be 1% of initial elastic modulus.

4. Example studies

4.1 Concentrically loaded short column

Since the concentric compressive test can reveal the basic mechanical performance of CFT, the major studies about CFT structures are focused on short column under concentric compressive load. Several groups of test about CFT short columns subjected to concentric compressive load are chosen as numerical examples. The details of those specimens are summarized in Table 1. The

Table 1 Properties of test specimens

Specimen	D (mm)	t (mm)	L (mm)	D/t	L/D	f_y (MPa)	E_s (Gpa)	f_c (MPa)	E_c (Gpa)	Reference
C2	141.4	6.50	608.0	21.8	4.3	313.0	206.01	23.81	23.53	Schneider (1998)
4HN	150.0	4.00	—	37.5	—	279.9	210.00	28.70	24.90	Susantha *et al.* (2001)
3MN	150.0	3.20	—	46.9	—	287.7	190.00	22.00	21.80	
4MN	150.0	4.00	—	37.5	—	279.9	210.00	22.00	21.80	
2LN	150.0	2.00	—	75.0	—	336.5	212.00	18.10	19.70	
3LN	150.0	3.20	—	46.9	—	287.7	190.00	18.10	19.70	
4LN	150.0	4.00	—	37.5	—	279.9	210.00	18.10	19.70	
CU022	140.0	6.50	602.0	21.53	4.30	313.0	—	23.80	—	Hu *et al.* (2003)
CU040	200.0	5.00	840.0	40.0	4.20	265.8	—	27.15	—	
CU047	140.0	3.00	602.0	47.0	4.30	285.0	—	28.18	—	
CU070	280.0	4.00	840.0	70.0	3.00	272.6	—	31.15	—	
CU100	300.0	3.00	900.0	100.0	3.00	232.0	—	27.23	—	
CU150	300.0	2.00	840.0	150.0	2.80	341.7	—	27.23	—	

Note: f_c = compressive strength of concrete, f_y = tensile strength of steel tube

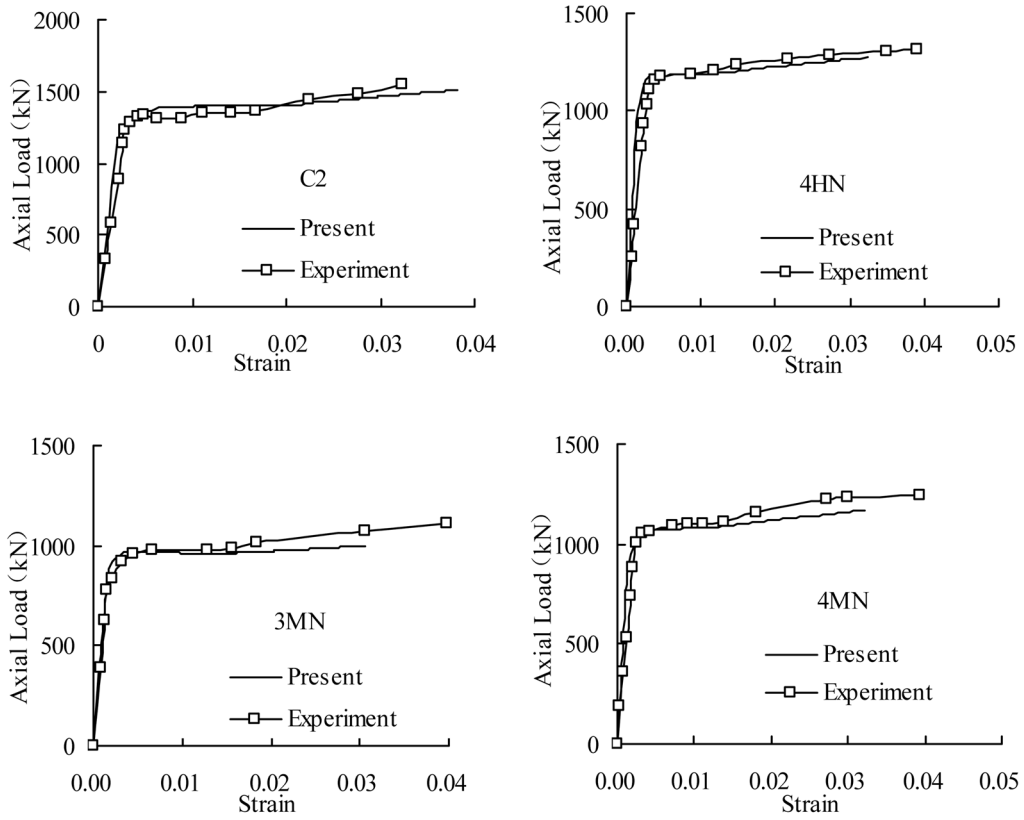

Fig. 3 Axial load versus axial strain for CFT short columns

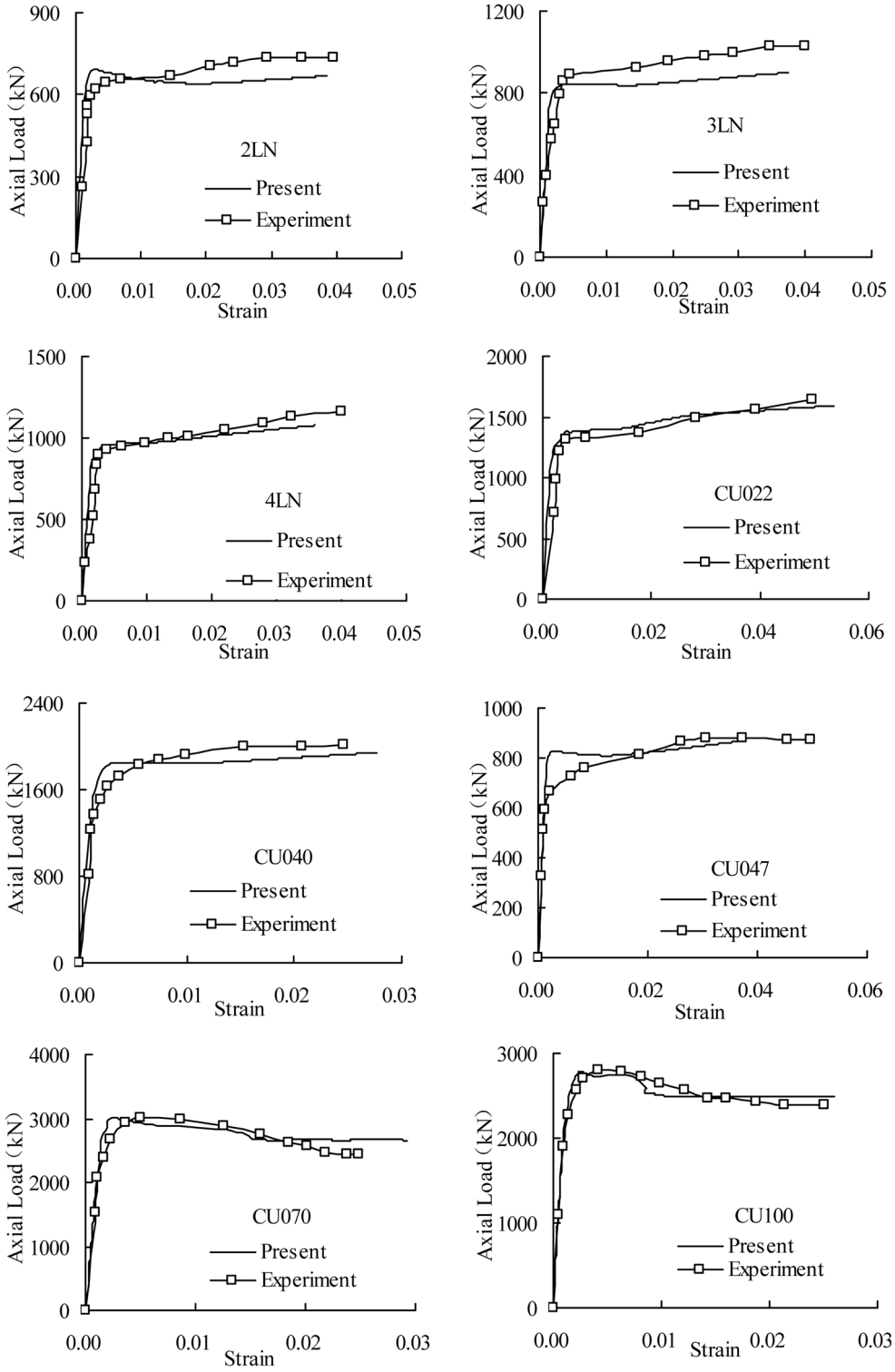

Fig. 3 Continued

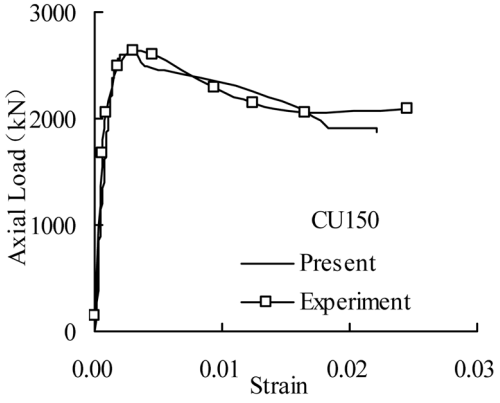

Fig. 3 Continued

experimental and numerical curves for axial load versus axial strain are plotted in Fig. 3, and good agreement can be observed. Generally, it has been widely accepted that the behaviors of CFT columns are mainly influenced by width-to-thickness ratio (*D/t*) of steel tube. From Fig. 3, it can be viewed that for the columns with *D/t* less than 40.0 (C2, 4HN, 4MN, 4LN and CU022), owing to strong radial pressure applied on the core concrete, obvious stain-hardening behavior can be observed both from experimental and numerical results. When *D/t* is not less than 70.0 (2LN, CU070, CU100 and CU150), significant strain-softening behavior is exhibited for CU070, CU100 and CU150. However, this softening behavior is not so obvious for 2LN. From Table 1, it can be found that although *D/t* of 2LN (75.0) and CU070 (70.0) is quite close, the value of f_y/f_c of 2LN (18.59) is far grater than that of CU070 (8.75), which may result in a more sustained radial constraint on core concrete after peak load for specimen 2LN. This phenomenon implies that the post-peak behavior of CFT is dependant not only on geometrical parameter (*D/t*) but also on material parameter (f_y/f_c). For the specimens with *D/t* between 40.0 and 70.0 (3MN, 3LN, CU040 and CU047), although some discrepancies exist between numerical and experimental results, the behavior of CFT columns can be approximately classified as elastic-perfectly plasticity.

4.2 Eccentrically loaded short column

For eccentrically loaded CFT columns, it has been aforementioned that with increment of eccentricity, the volume expansion of core concrete may decrease gradually, which will weak the confining pressure acted on core concrete. In the present study, a reduction parameter α is introduced in Eqs. (16) and (17) to consider the influence of eccentricity on confining stress. It can be found from Eq. (17) that when eccentricity e is equal to 0, which implies that the load is concentrically applied, α is taken as 1.0. For the column subjected to eccentrical load, α will decrease gradually with e. When e is greater than $D/2$, α is assumed to be zero, which means no confining pressure is applied on core concrete, and the behavior of core concrete is similar to that of normal unconfined concrete. With the modified confining pressure model, three tests about eccentrically loaded CFT column (Tang *et al.* 1982, Cai 2003, Matsui *et al.* 1995), which denote as specimen A1, A2, and A3, respectively, are investigated, and *M-N* interaction envelopes are plotted in Fig. 4. To give a more clear inspection about this topic, the numerical results for $\alpha = 0.0$ and 1.0

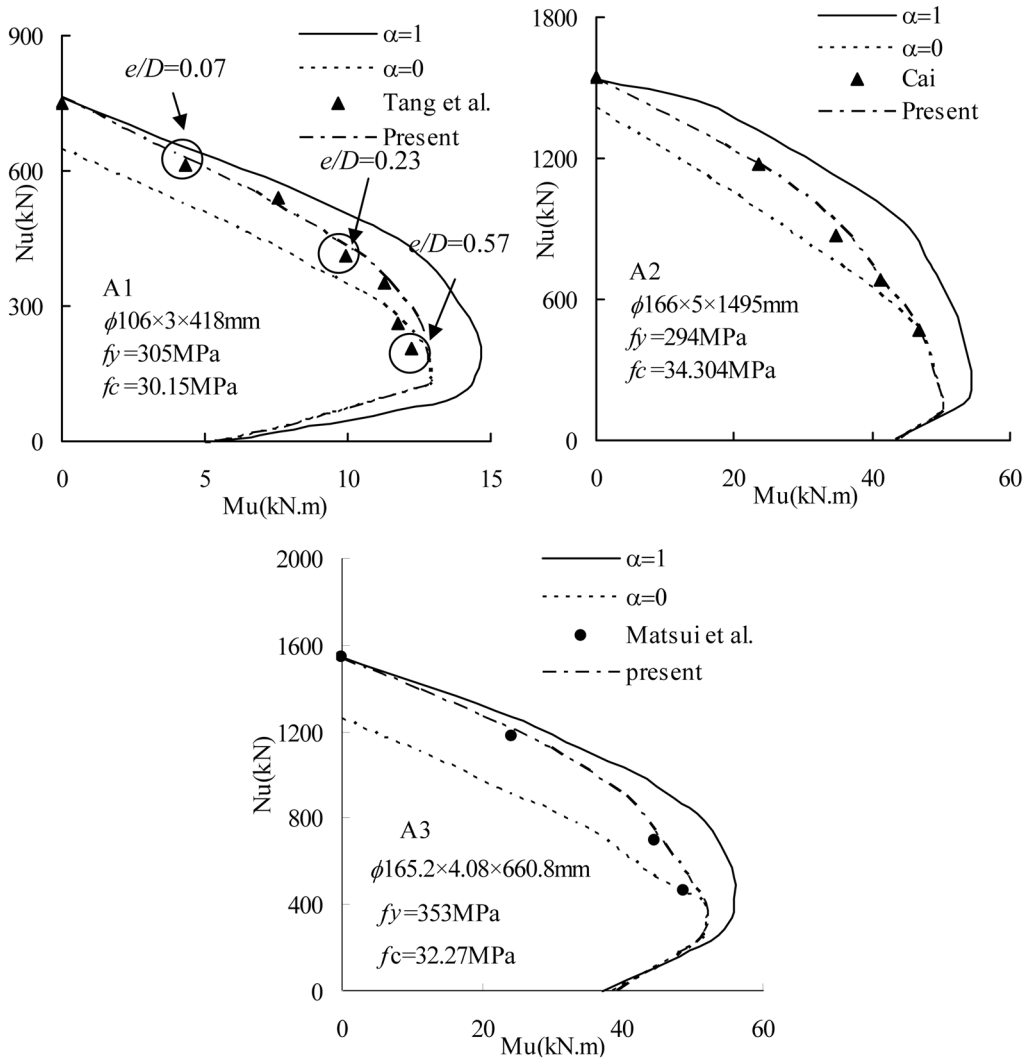

Note: f_c = compressive strength of concrete, f_y = tensile strength of steel tube

Fig. 4 *M-N* interaction curve for eccentrically loaded CFT

are also given. From Fig. 4, it can be viewed that the results of proposed model agree with experimental results well. Moreover, it can be found that the numerical results for $\alpha = 1.0$ and 0.0 can be viewed as the upper and lower boundaries for experimental results. When the column is concentrically loaded or e is comparably small, the experimental results are located near the curve of $\alpha = 1.0$ (completely confined concrete). With increment of e (M/N), the test points approach the curve of $\alpha = 0.0$ (unconfined concrete) gradually.

To give a further mechanical explanation about the phenomenon illustrated in Fig. 4, for specimen A1, Fig. 5 presents the sectional stress distribution of core concrete under failure when $e/D = 0.07$, 0.23, and 0.57. From Fig. 5, it can be found that for $e/D = 0.07$ (small eccentrically loaded column), the core concrete is under whole-section compression. Therefore, it can be deduced that the

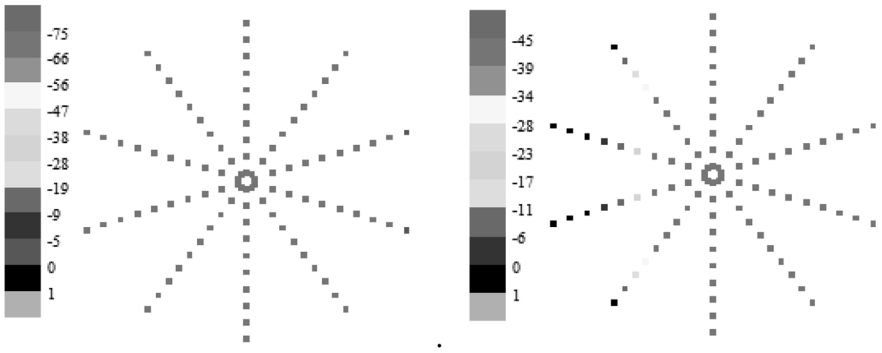

(a) *e/D*=0.07 (b) *e/D*=0.23

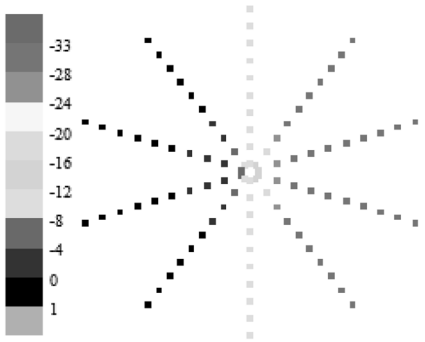

(c) *e/D*=0.57

Fig. 5 Stress distribution of core concrete

confining pressure applied on core concrete may be similar with that of axial loaded CFT column. On the contrary, when $e/D = 0.57$ (large eccentrically loaded column), a large portion of core concrete has been tensile cracked, and trivial confining pressure can be predicted. The case of $e/D = 0.23$ can be viewed as an intermediate state between small and large eccentrically loaded column, and a reduction of confining pressure may be an appropriate way to reflect the actual behavior.

4.3 Slender column

For slender columns, especially when eccentrical or transverse load is applied, geometrical nonlinearity will occur due to large deformation. The experimental tests for eccentrically loaded CFT slender columns executed by Zeghiche *et al.* (2005) are studied. The results of relation between load and mid-height transverse deflection are shown in Fig. 6. To investigate the influence of geometrical nonlinearity (GN), the results that only material nonlinearity is involved are also given. It can be observed from Fig. 6 that the behaviors of columns before peak can be well predicted by the proposed model with geometrical nonlinearity. It seems that the deviation from the experiment curve after peak may be account for the difficulty of load controlling in experiment

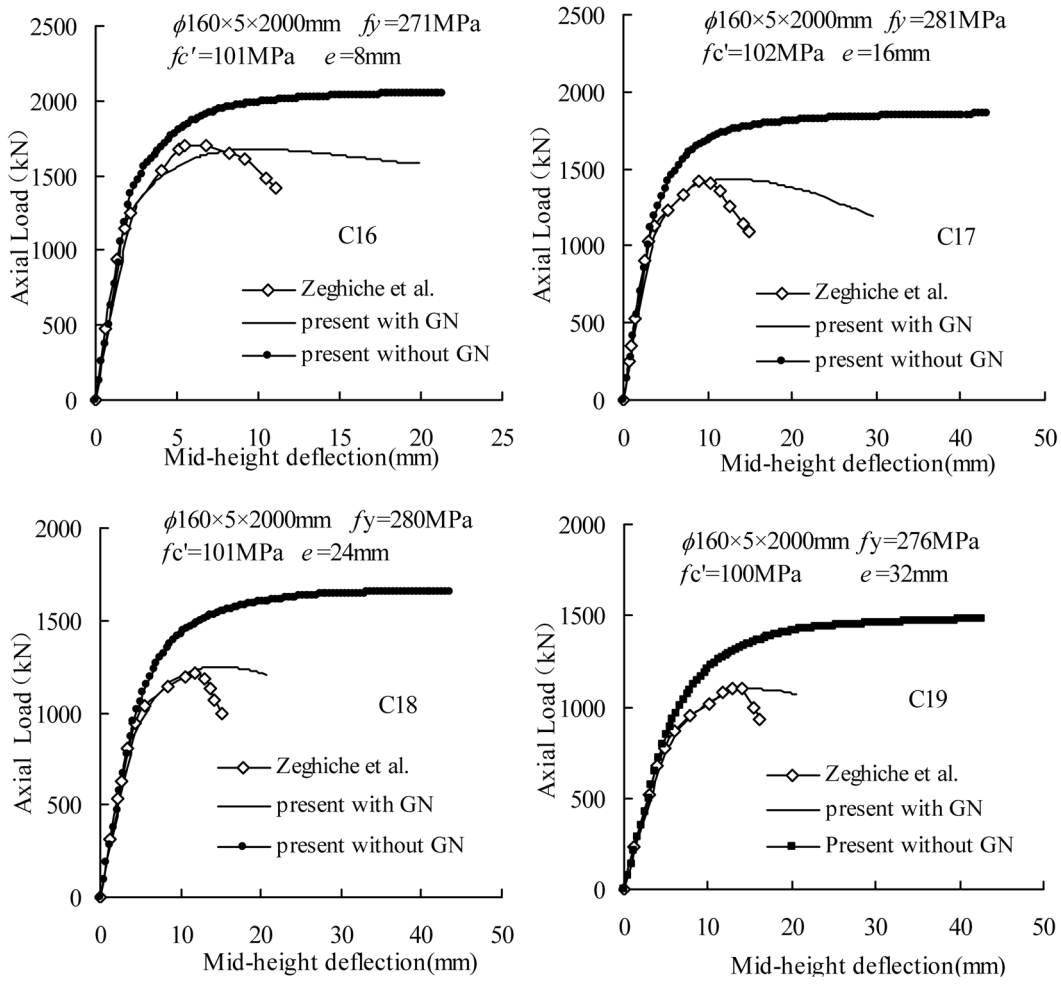

Note: $f_c^{'}$ = cylinder compressive strength of concrete, f_y = tensile strength of steel tube

Fig. 6 Axial load versus mid-height deflection of eccentrically loaded slender column

during softening period. Moreover, it can also be found that if the geometrical nonlinearity is not involved, the resistance capacity will be obviously overestimated.

The sectional stress distribution of specimen C19 under failure is plotted in Fig. 7. It should be worth to notice that geometrical nonlinearity has significant influence on the failure mode of eccentrically loaded CFT column. If no geometrical nonlinearity occurs (i.e., short column), the whole section is under compression, and the failure can be attributed to crushing of core concrete. However, for slender column, owing to large transverse deflection, a secondary moment will be introduced, and crack of concrete can be obviously observed.

A group of CFT columns with slenderness ratio ($\lambda = 4L/D$) varied from 32 to 96 is comprehensively tested by Matsui *et al.* (1995). The experimental and numerical results of *M-N* interaction envelopes are illustrated in Fig. 8, and excellent agreement can be observed. In Fig. 8, due to perturbation and truncation error in numerical computation, which should amplify the geometrical nonlinear effect, meaningful numerical solution for concentric compressive test is

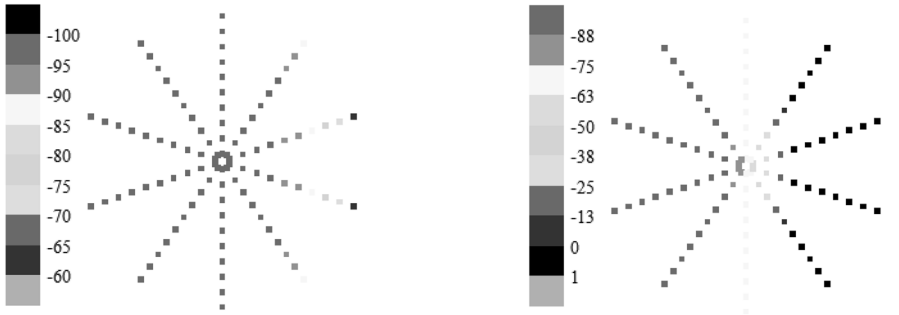

(a) Geometrical nonlinearity is not involved **(b) Geometrical nonlinearity is involved**

Fig. 7 Sectional stress distribution of C19 under failure

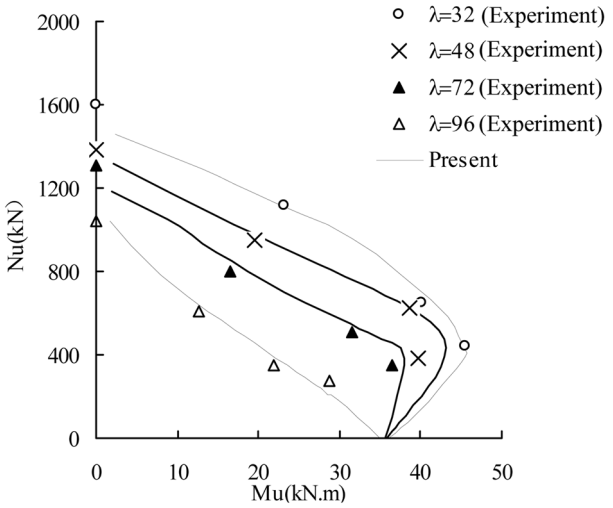

Fig. 8 *M-N* interaction curve for eccentrically loaded CFT ($D \times t = 165.2 \times 4.08$ mm)

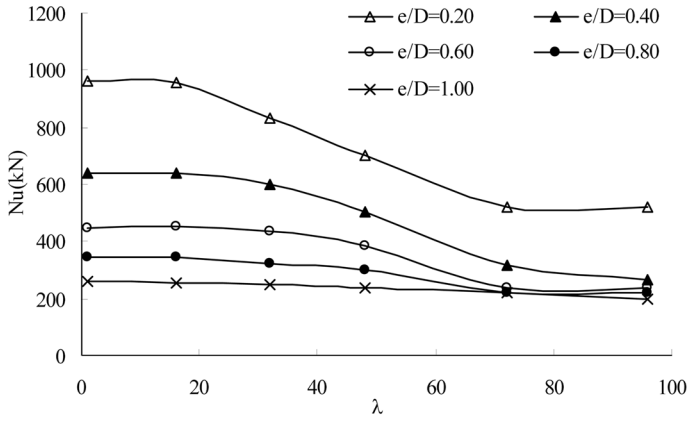

Fig. 9 The relation between axial resistance capacity and slenderness ratio

difficult to obtained, therefore, no corresponding numerical results are presented. However, it can be observed that with decrease of eccentricity, the curve of numerical simulation approach test points gradually. Moreover, it is quite interesting to find that, for column with $\lambda = 96$, the shape of *M-N* interaction curve is distinctively different from that of other columns, which may imply that with increment of slenderness ratio λ, the secondary moment caused by geometrical nonlinearity can significantly accelerate the collapse of slender columns. In Fig. 9, the relations between axial resistance capacity and slender ratio subjected to different eccentricity are presented. From the results, it can be found with increment of slenderness, the axial resistance capacity of small eccentrically loaded columns (e.g., $e/D = 0.2$, 0.4 and 0.6) should be decrease enormously due to geometrical nonlinearity. However, for large eccentrically loaded cases (e.g., $e/D = 0.8$ and 1.0), an almost flat curve is observed, and this phenomenon may imply that bending moment will control the failure of column for large eccentrically loaded columns, and the secondary effect caused by large deformation is undermined.

4.4 Arch

During the past two decades, CFT has been widely used as arch rib in bridge engineering. For example, Wushan Yangzhi Bridge in China has a CFT rib with span of 440 m. Generally, the arch rib is subjected to combining action of axial force and moment. Unlike CFT columns, the compressive eccentricity of arch is implicit and is not a constant value along arch axis. In the present study, a linear FEM analysis will be carried in prior, and the eccentricity of every element is obtained through linear analysis result of *M*/*N*.

An experiment of CFT arch carried by Chen *et al.* (2002) is studied. The geometrical configuration and material properties are shown in Fig. 10. The curve of inner edge of arch is given as

$$Y = X^2/3.45 \tag{24}$$

in which the coordinates X and Y are defined through the way illustrated in Fig. 10.

Two load cases, i.e., Case 1 and Case 2, are carried in the experiment. In Case 1, a vertical concentrated load is applied at crown (Point A). In Case 2, the concentrated load is applied at 1/4 span (Point B). The results of vertical displacement of arch are given in Fig. 11, and agreement

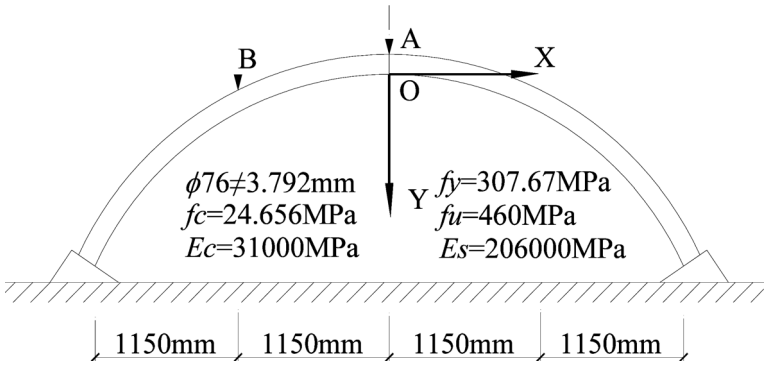

Fig. 10 Geometrical configuration and material properties of CFT arch

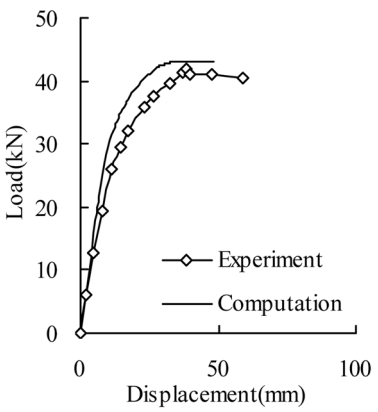

(a) Half span (Point A)

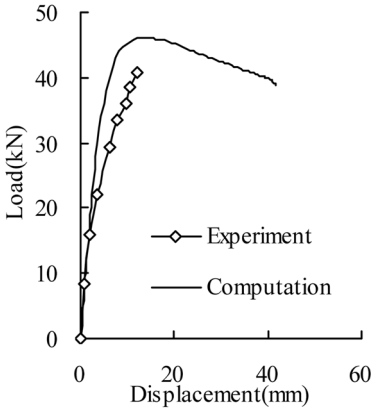

(b) 1/4 span (Point B) and 3/4 span

Case 1

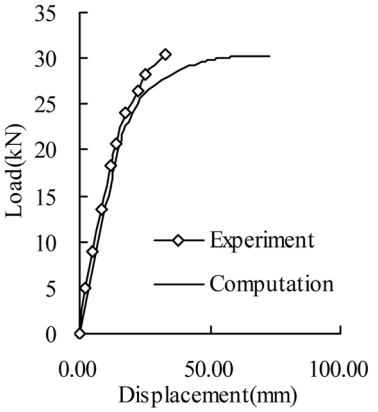

(a) 1/4 span (Point B)

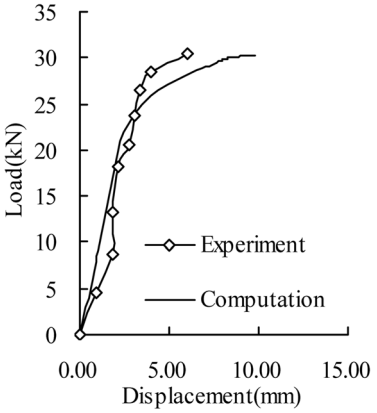

(b) 1/2 span (Point A)

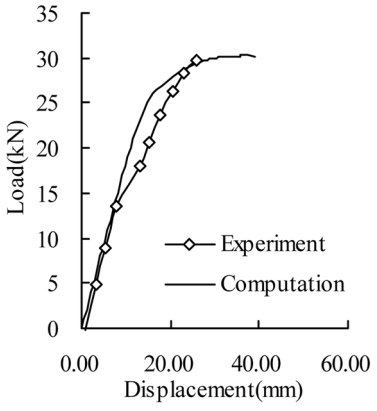

(c) 3/4 span

Case 2

Fig. 11 Vertical displacement of CFT arch

between experiment and numerical results can be observed.

Fig. 12 gives the stress distribution of core concrete of 1/4 span section and crown section under failure, and an obvious crack of core concrete can be viewed. Therefore, in can be deduced that for the experimental load cases the confining effect of steel tube on core concrete may be comparably weak. As comparison, the results of failure stress distribution of core concrete under whole-span uniform distributing load case, which is not carried in experiment, are also presented in Fig. 13. It can be found that for 1/4 span section, the whole section of core concrete is under compressive, and for half span section, only a small portion of core concrete cracked. It can be concluded that under whole-span uniform distributing load case, comparably strong confining pressure can be predicted in CFT arch rib.

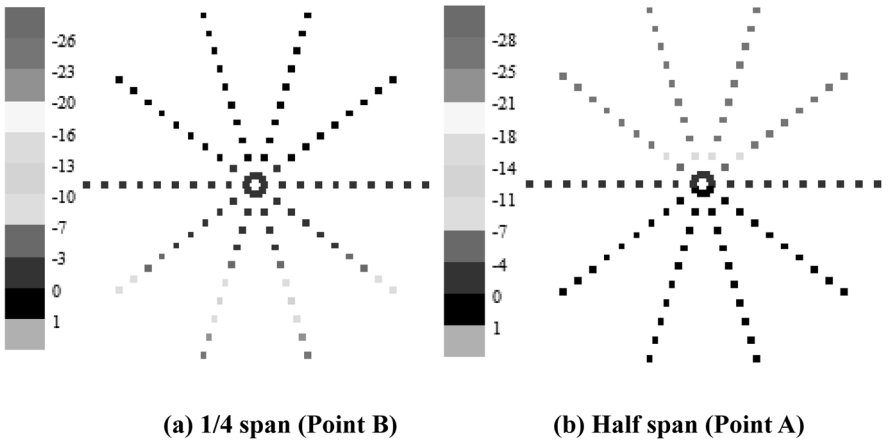

(a) 1/4 span (Point B) **(b) Half span (Point A)**

Case 1

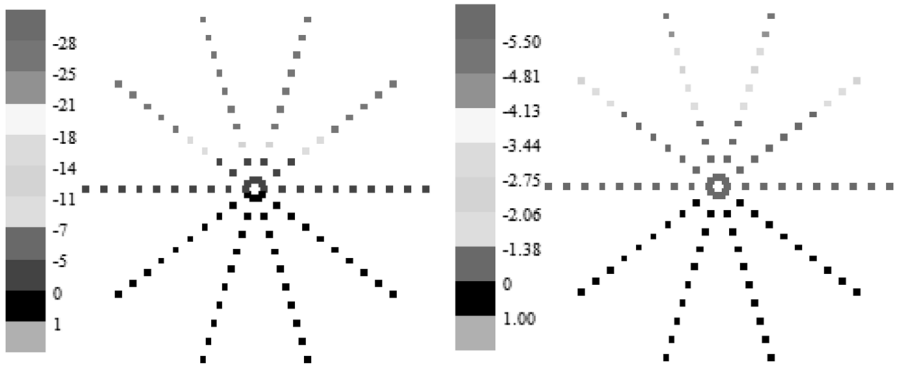

(a) 1/4 span (Point B) **(b) Half span (Point A)**

Case 2

Fig. 12 Stress distribution of core concrete under Case 1 and 2

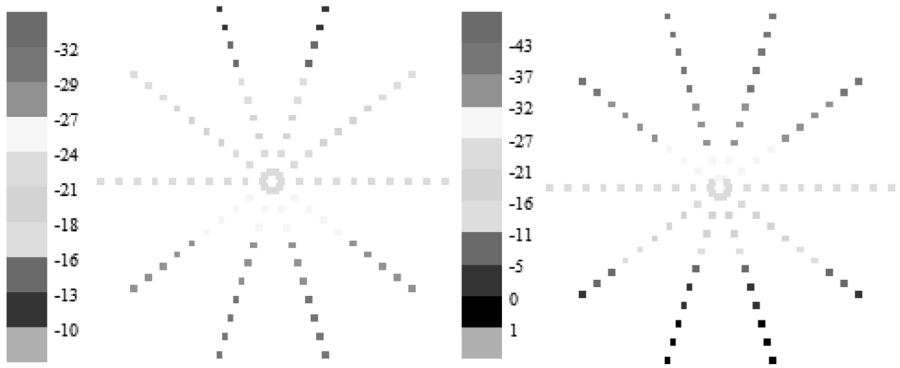

(a) 1/4 span (Point B) **(b) Half span (Point A)**

Fig. 13 Stress distribution of core concrete under whole span uniform distribution load

5. Conclusions

The mechanical behaviors of CFT structure are investigated by nonlinear FEM analysis. The degenerated beam element is adopted in numerical simulation. Based on those previous experimental studies, some modifications about stress-strain relationship of core concrete, which include a reducing parameter on confining stress caused by eccentricity and a numerical model for descending branch, are proposed. Updated Lagrange formulation is used to describe the large deformation effect. From the study results, the following conclusions can be drawn.

(1) In the present study, some modifications about constitutive model of confined concrete are proposed, and numerical consistence and extension of the proposed model are emphasized. The structural behaviors of concentrically loaded CFT columns with D/t varied from 21.8 to 150 are investigated, and the resistance capacity and ductility are well predicted.

(2) For eccentrically loaded CFT columns, the confining stress should be reduced gradually with eccentricity, and this effect can be described effectively by a reduction parameter, which is illustrated in Eqs. (16) and (17).

(3) For CFT slender columns, the secondary moment caused by large deformation may weak the confining effect, and the failure mode may be quite different with that of CFT short columns.

(4) For CFT arch, considering that the eccentricity is implicit and is not a constant value along arch axis, it can be found that the confining effect in arch structure is more complicated and variable than that in columns. To obtain a whole comprehension and inspection about mechanical behaviors of CFT arch, further intensive researches with nonlinear FEM is strongly recommended.

Acknowledgements

The research reported in this paper was financially supported by Doctoral Fund for Youth Scholars of Ministry of Education of China (No. 20090184120033) and the Fundamental Research Funds for the Central Universities. The support is gratefully acknowledged.

References

Ahmad, S., Irons, B.M. and Zienkiewicz, O.C. (1970), "Analysis of thick and thin shell structures by curved finite elements", *Int. J. Numer. Meth. Eng.*, **2**, 419-451.

Bathe, K.J. and Bolourchi, S. (1980), "A geometrical and material nonlinear plate and shell element", *Comput. Struct.*, **11**, 23-48.

Cai, S.H. (2003), *Modern Steel Tube Confined Concrete Structures*, China Communications Press Co., Beijing, China. (in Chinese)

Chen, B.C., Ou, Z.P., Wang, L.Y. and Han, L.H. (2002), "Experimental study on carrying capacity of concrete filled steel tubular column under eccentric load", *J. Fuzhou Univ.*, **30**(6), 838-844. (in Chinese)

Chen, B.C., Chen, Y.J., Wang, L.Y. and Han, L.H. (2004), "Study of stress-strain relation of concrete filled steel tubular eccentric compression column", *China J. Highw. Transp.,* **17**(1), 24-28. (in Chinese)

Elremaily, A. and Azizinamini, A. (2002), "Behavior and strength of circular concrete-filled tube columns", *J. Constr. Steel Res.*, **58**, 1567-1591.

Fujimoto, T., Mukai, A., Nishiyama, I. and Sakino, K (2004), "Behavior of eccentrically loaded concrete-filled steel tubular columns", *J. Struct. Eng-ASCE*, **140**(2), 203-212.

Gupta, PK., Sarda, S.M. and Kumar, M.S. (2007), "Experimental and computational study of concrete filled steel tubular columns under axial loads", *J. Constr. Steel Res.*, **63**, 182-193.

Han, L.H. (2004), "Flexural behavior of concrete-filled steel tubes", *J. Constr. Steel Res.*, **60**, 313-337.

Hu, H.T., Huang, C.S., Wu, M.H. and Wu, Y.M. (2003), "Nonlinear analysis of axially loaded concrete-filled tube columns with confinement effect", *J. Struct. Eng-ASCE*, **129**(10), 1322-1329.

Hu, H.T., Huang, C.S. and Chen, Z.L. (2005), "Finite element analysis of CFT columns subjected to an axial compressive force and bending moment in combination", *J. Constr. Steel Res.*, **61**, 1692-1712.

Huang, C.S., Yeh, Y.K., Liu, G.Y., Hu, H.T., Tsai, K.C., Weng, Y.T., Wang, S.H. and Wu, M.H. (2002), "Axial load behavior of stiffened concrete-filled steel columns", *J. Struct. Eng.*, **128**(9), 1222-1230.

Marques, J.B. and Caldas, R.B. (2005), "Numerical analysis of composite steel-concrete columns of arbitrary cross section", *J. Struct. Eng-ASCE*, **131**(11), 1721-1730.

Matsui, C., Tsuda, K. and Ishibashi, Y. (1995), "Slender concrete filled steel tubular columns under combined compression and bending", *Structural Steel: PSSC'95-4th Pacific Structural Steel Conference*, Steel-Concrete Composite Structures, Vol. 3, Singapore.

Mirza, S.A., Hyttinen, V. and Hyttinen, E. (1996), "Physical tests and analyses of composite steel-concrete beam-columns", *J. Struct. Eng-ASCE*, **122**(11), 1317-1326.

Parisch, H. (1981), "Large displacements of shells including material nonlinearities", *Comput. Method. Appl. M.,* **27**, 183-214.

Saenz, L.P. (1964), "Equation for the stress-strain curve of concrete", *ACI J.*, **9**(61), 1229-1235.

Schneider, S.P. (1998), "Axially loaded concrete-filled steel tubes", *J. Struct. Eng.*, **124**(10), 1125-1138.

Susantha, K.A.S., Ge, H.B. and Usami, T. (2001), "Uniaxial stress-strain relationship of concrete confined by various shaped steel tubes", *Eng. Struct.*, **23**, 1331-1347.

Tang, G.Z., Zhao, B.Q., Zhu, H.X. and Shen, X.M. (1982), "Study on the fundamental structural behavior of concrete filled steel tubular columns", *J. Build. Struct.*, **3**(1), 13-31. (in Chinese)

Worsak, K.N. (1978), "A simple and efficient finite element for general shell analysis", *Int. J. Numer. Meth. Eng.*, **14**, 179-200.

Xiang, T.Y., Tong, Y.Q. and Zhao, R.D. (2005), "A general and versatile nonlinear analysis program for concrete bridge structure", *Adv. Eng. Softw.*, **36**, 681-690.

Zeghiche, J. and Chaoui, K. (2005), "An experimental behavior of concrete-filled steel tubular columns", *J. Constr. Steel Res.*, **61**, 53-66.